RILEM Technical Letters (2024) 9: 117-126
https://doi.org/10.21809/rilemtechlett.2024.205

Field measurements of galvanic anode cathodic protection of reinforced concrete systems in marine environment: Influence of water level and biofilm

Deeksha Margapuram[1,2,*], Marie Salgues[2], Océane Thibault[3], Raphaël Lami[3], Benjamin Erable[4], Michel Groc[5], Renaud Vuillemin[5], Bruno Hesse[5], Jean-Claude Souche[2], Florian Stratta[2], Marine Bayle[6], Jean-Bernard Memet[6], Laurent Zudaire[5], Fabrice Deby[1], Stéphane Laurens[7], Chantal Chalhoub[7], Elie Sassine[7], Fabien Nougarolles[1], Deepak Kumar Kamde[1], Alexandra Bertron[1]

[1]LMDC, Université de Toulouse, UPS, INSA, Toulouse, France
[2]LMGC, IMT Mines Alès, University of Montpellier, CNRS, Alès, France
[3]Sorbonne Université, UPVD, CNRS, Laboratoire de Biodiversité et Biotechnologies Microbiennes, LBBM, F-66650 Banyuls-sur-Mer, France
[4]Laboratoire de Génie Chimique, Université de Toulouse, CNRS, INPT, UPS, Toulouse, France
[5]Sorbonne Université, CNRS, - REMIMED FR3724, Observatoire Océanologique de Banyuls, Banyuls-sur-Mer, France
[6]A-Corros Expertise, Arles, France
[7]Corrohm, Labège, Toulouse, France

Received: 25 November 2024 / Accepted: 11 March 2025 / Published online: 17 March 2025

Abstract

Corrosion of steel in concrete is one of the major deterioration mechanisms for reinforced concrete (RC) structures such as floaters of floating offshore wind turbines (FOWTs). As these are vital components of FOWTs, addressing corrosion is critical to ensure their durability with minimal maintenance. The existing literature indicates that RC in the tidal zone can experience premature corrosion. To mitigate this, galvanic cathodic protection (CP) is a well-known approach for protecting RC structures. Therefore, a field experiment in the tidal zone was conducted to study the behaviour of aluminum anode CP for RC with CEM I and CEM V cement types across two concrete surface textures, smooth and rough. The half-cell potentials (HCP) (for specimens without CP), mixed potentials and protection current (for specimens with CP) were monitored continuously. Furthermore, the effect of water levels and biofilm on corrosion characteristics of steel in concrete and the efficiency of CP was assessed. The findings highlighted that the biofilm on the concrete surface acts as a physical barrier, limiting the diffusion of oxygen – affecting the corrosion characteristics of steel embedded in concrete. This influence was distinctly observed in both protected and non-protected categories. In the protected category, the average protection current was found to increase upon biofilm removal for CEM I concrete - indicating that the CP is efficient/or working with or without biofilm on the concrete surface. Finally, this paper highlights the importance of understanding how the presence of biofilm on concrete surfaces can affect the corrosion characteristics of steel embedded in concrete.

Keywords: Galvanic anode cathodic protection; Reinforced concrete; Water level; Biofilm; Tidal zone.

1 Introduction

Floating offshore wind turbines (FOWTs) are designed to generate clean power using wind energy, a renewable source. This technological advancement of FOWTs support global efforts to mitigate climate change by minimizing greenhouse gas (GHG) emissions. As energy demands shift towards renewable sources, FOWTs are increasingly preferred over standard fixed-bottom turbines, especially in deep-water locations, ranging between 50 and 200 m water depth [1]. These locations have strong and reliable winds, allowing for higher amounts of energy generation, and are away from the shoreline. Moreover, the extreme conditions such as high wind speeds and strong tidal currents prevailing in these locations pose a challenge to components of FOWT. Among all the components, the foundation (also known as floater) is primarily constructed using steel due to its high strength, ease of fabrication, and its capacity to offer structural integrity to withstand extreme offshore conditions. Despite the benefits of using steel in floaters, they exhibit corrosion in harsh marine environments [2]. As a result, reinforced concrete (RC)

*Corresponding author: Deeksha Margapuram, E-mail: margapuram@insa-toulouse.fr

floaters could be a promising alternative to steel floaters. They can be designed for enhanced durability (with a possibility of designing a long corrosion-free service life) with fatigue resistance at low production and maintenance costs, making it an economical and sustainable option [3]. However, RC infrastructure may exhibit premature corrosion of embedded steel especially in the tidal zone. It is due to the cyclic wetting and drying cycles, significantly influencing the service life and durability of RC in these conditions [4]. The service life of RC structures is defined as the period during which it performs its function it was designed for while meeting the consumer's requirements. This process occurs in three stages: corrosion initiation, corrosion propagation, and repair. Perhaps most importantly, for RC floaters, maintaining an extended service life involves delaying corrosion initiation, and prolonging the initial phase of propagation. This can be achieved by using supplementary cementitious materials (SCMs) such as slag, fly ash, etc., which increase concrete resistivity and reduce corrosion rate. Additionally, the use of SCMs is well-known for their capacity to refine pore structure and reduce permeability, thereby enhancing the durability of RC in marine environments [5], [6]. For instance, the long-term field investigation by Kwon et al. [7] reported that the cement blends incorporating SCMs demonstrate effective resistance to corrosion of RC systems and may lead to durable RC systems in marine environments. They also indicate that the formation of calcareous deposits on the exposed concrete surface – leading to reduction in the porosity of concrete and the corrosion rate of embedded steel. However, the authors could not find any literature focusing on the effect of the presence of micro- and macro-fouling on concrete surface and its underlying effect on corrosion of embedded steel in concrete. Biofilm formation, a natural process occurs on any material immersed in seawater. The development of biofilm on the surface of cementitious substrates in marine environments depends on the intrinsic properties of the substrate such as surface roughness, binder chemistry, substrate pH, and external environmental conditions [8], [9], [10]. Surface roughness is a critical intrinsic factor influencing the rate of microbial colonization. For example, some authors demonstrated that rough surfaces exhibit higher initial biocolonization rate than smooth-textured concrete surfaces [11], [12]. As a result, a part of this research is dedicated to this aspect by creating smooth and rough RC exposure surfaces. This represents the state-of-the-art approach by integrating biodiversity considerations into the design of durable concrete structures in the marine environment. Note that the formation of biofilm on a substrate is divided into two categories, microfouling (bacteria and microalgae) and macrofouling. Due to the high relative humidity and exposure to seawater tides in the tidal zone, floaters that are occasionally partially submerged are subjected to these conditions, resulting in a moist, nutrient-rich environment, suitable for the proliferation of microorganisms.

Biofilms have been proven to form a protective, physical barrier on steel, minimizing direct contact between corrosive agents (for example, chlorides and sulphate ions) with the underlying steel [13], [14]. This layer could reduce the rate of corrosion by limiting the contact of aggressive ions from seawater. Similarly, in the case of RC, biofilm on the concrete surface may restrict the entry of these ions and/or gases, potentially influencing the corrosion characteristics of steel in concrete. To address the existing knowledge gap regarding the influence of biofilm on the electrochemical characteristics of steel embedded in concrete with and without SCMs, this research study aims for a detailed investigation.

Considering that the FOWTs are structures of high importance, the corrosion protection of embedded steel is essential and can be done by using cathodic protection (CP), a widely known protection strategy for RC structures. To protect steel in concrete, CP can be implemented either by impressed direct current and/or by attaching a galvanic anode to the steel rebars. The use of CP facilitates shifting the electrochemical potential of steel in concrete to control corrosion. For CP with galvanic anodes, the more electronegative metals such as zinc, aluminum, and magnesium can be connected to embedded steel in concrete before or after the initiation of corrosion of steel. Much information is available on the effect of binder type, relative humidity, anode-to-cathode ratio, rebar location, etc. on the performance of CP of steel in concrete [15], [16], [17]. However, the effect of the presence of biofilm on concrete surfaces on the effectiveness of galvanic anode is not reported. Therefore, this research study addresses the effect of water level and biofilm development on (i) the corrosion characteristics of steel embedded in concrete with CEM I and low-carbon-based CEM V cement types under both protected and non-protected conditions, and (ii) the effectiveness of galvanic CP. Furthermore, the findings presented in this study is a part of an ongoing long-term field investigation aimed at understanding the CP performance for marine-exposed RC FOWTs.

2 Research significance

The longevity of RC floaters for FOWTs is critical for the long-term development of the offshore wind sector. These floaters in the tidal zone face several challenges due to the aggressive ions in seawater, biofouling, and other marine environmental conditions. To protect them, one of the possibilities is the use of CP with a galvanic anode, such as aluminum metal, well-suited for marine environment (ISO 12696:2012) [18]. This study presents the influence of biofilm and varying water levels on the corrosion characteristics of embedded steel in concrete with CEM I (low resistivity) and CEM V (high resistivity). This work highlights the significance of biofouling on corrosion and its control using galvanic anodes for durability of reinforced concrete structures.

3 Materials and methods

To evaluate the effect of water level and biofilm formation on the performance of galvanic anode CP of steel embedded in concrete with different binders, three replicas of the following type of specimens were prepared: (i) CEM I with smooth exposure surface of concrete, (ii) CEM V with smooth exposure surface of concrete, and (iii) CEM V with rough exposure surface of concrete. CEM I was selected as the reference binder due to its large usage and well-documented

properties, providing a reliable baseline for comparison. At the same time, new age RC structures are being built with the use of low carbon binders such as CEM V. Therefore, this was essential to understand the effect of roughness in the latter's case. Besides, a critical gap remains in understanding how CEM V binder, characterized by high concrete resistivity, interacts with galvanic anode cathodic protection (CP) systems exists.

3.1 Description of reinforced concrete block specimens

Figure 1A shows the arrangement of steel rebars (arranged in grid pattern) and reference electrode (RE) in a wooden mold. For each specimen, steel rebars of nominal diameter (ϕ) 20 mm were cut to a length of 160 mm (a total of four) and arranged in a grid pattern by welding the intersections. The steel reinforcement was then placed in a wooden mold with internal dimensions of (200 × 200 ×110) mm. The concrete cover was designed to be 50 mm (like that used for RC structures exposed in marine environments). The steel reinforcement was used "as received" by the supplier, with mill scale intact and no visible corrosion spots, to simulate real-world conditions. Please note that the the steel complies with standards EN 10079 [19] and NF EN 10080 [20], which define its suitability for welding without alteration to its microstructure/minerology. A piece of cotton cloth was used to clean the reinforcement, removing any dust or loose foreign elements, if present. Two bolts were welded to opposite sides of the rebars to connect electrical cables (see Figure 1A). This welded area, along with the nuts, bolts, and washers, was covered with a thick layer of epoxy resin to electrically insulate this area. To secure each RC block to the grating panel (details in Section 2.2), two 180-mm long PVC pipes with side plugs were nailed to opposite sides of the box. As shown in Figure 1A, a commercially available embeddable manganese dioxide RE was positioned close to the rebar using self-locking plastic straps. It was sourced from Force Technology, Denmark. The average potential of MnO_2 reference electrode is + 216 mV vs. Ag/AgCl. This was selected for this study due to its design for monitoring steel corrosion in concrete and its long-term stability, with a reported durability of over 10 years [21]. To further ensure consistency in potential measurements, the potential of embedded rebars were measured using an external Ag/AgCl electrode once in six months. Then, the potential of rebars against Ag/AgCl and embedded MnO_2 reference electrodes were compared to confirm their functioning and accuracy in measurements.

This study used two types of cement to cast RC blocks: CEM I 52.5 N - SR 5 CE PM-CP2 NF (CEM I) and CEM V/A (S-V) (CEM V) (supplied by *Lafarge* and *Ciments Calcia Heidelberg,* respectively). The concrete mix (see Table 1) was prepared with water-to-binder ratio of 0.5. The aggregates and sand were both siliceous alluvial in nature. The RC blocks were demolded after 36 hours and cured in the curing room at a RH of 60±5%, and a temperature of 20°C for 28 days and 56 days for CEM I and CEM V respectively. Regarding the difference in curing time, the curing duration for CEM V was extended to 56 days to ensure that its compressive strength at this stage closely reflects its final strength. Since CEM V exhibits a slower hydration process, this extended curing period allows it to achieve mechanical performance comparable to that of CEM I at 28 days. Then, epoxy resin was applied to all sides of the RC block, except the exposed surface, to ensure unidirectional ingress of chemical ions. Furthermore, the exposed surface is separated into two textures: smooth and rough, particularly for CEM V. A soft silicon mold with microscale peaks and valleys was used for creating a rough texture similar to a natural rock substrate (as shown in Figure 1C). In this research study, smooth and rough surfaces refer to surfaces cast with/without silicon mold. Smooth surfaces refer to RC specimens with uniform texture free of visible irregularities. Rough surfaces refer to RC specimens with inherent microtexture from silicon mold used. These surfaces are unmodified post-casting to replicate real-world conditions.

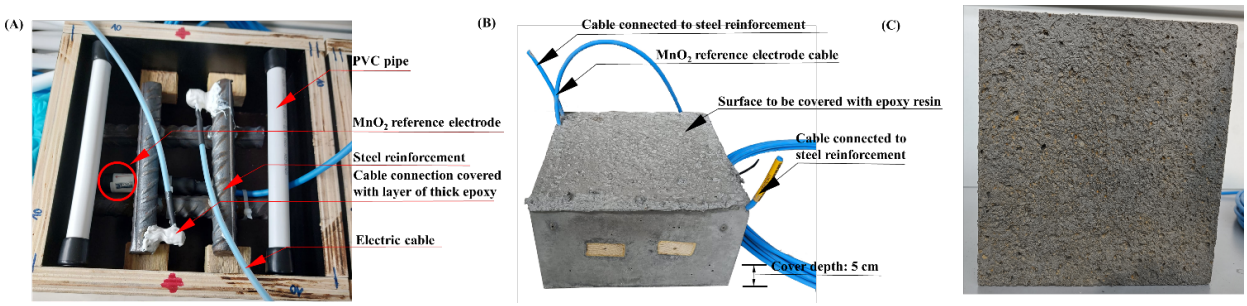

Figure 1. (A) Wooden formwork with different components in the RC block including a grid-shaped steel reinforcement and two PVC pipes on the opposite sides to suspend it on a grating panel and manganese dioxide reference electrode (circled in red) for continuous monitoring of electrochemical potential of embedded steel reinforcement (B, C) Photograph of RC block and surface having a rough texture.

Table 1. Concrete mix design used in this study for 1 m^3 of concrete.

Type of cement	Binder (kg)	Sand (kg)	Aggregates (kg)	Effective water (kg)
CEM I - smooth	385	823	1024	158
CEM V - smooth	385	799	1000	170
CEM V - rough	385	839	1011	119

3.1.1 Properties of concrete

To investigate the properties of concrete, three unreinforced concrete specimens were prepared for each binder type, CEM I and CEM V. The following tests were conducted after 56 days of curing period as they would represent the long-term performance, particularly for this application. The findings reported next are an average of three unreinforced specimens. The average resistivities of CEM I and CEM V concrete were 151 Ωm and 304 Ωm (as per AFNOR, XP P 18-481) [22], respectively. The average water accessible porosity (NF P 18-459) [23] measurements for CEM I and CEM V concrete were 16.12 % and 17.35 %, respectively. The total charge passed (measured using the Rapid Chloride Permeability Test (RCPT) as per ASTM C1202) [24] for CEM V concrete was measured to be 582 Coulombs, which is six times lower than CEM I concrete (3479 Coulombs).

3.2 Configuration of RC block specimens without and with galvanic CP

Figure 2A shows that a total 15 number of RC blocks (six without and nine with galvanic CP). For the RC blocks without CP, three grating panels were arranged, each containing two blocks with CEM I (smooth texture), CEM V with smooth, and CEM V with rough textures on the exposed surface. A similar arrangement was followed for the RC blocks with galvanic CP, but with three blocks per grating panel, and an external aluminum anode was connected to each panel, meaning one Al galvanic anode was shared with three RC blocks. The external anode was positioned in seawater at a depth of ~ 500 mm from the centre of the grating panel (as shown in Figure 2B)

Electrical cables from all RC blocks were connected to a data logger to monitor the electrochemical potential of each at an interval of 15 minutes. Connections between the external aluminum anode and steel reinforcement (cathode) cables were integrated with a data acquisition system. For blocks without CP, half-cell potentials of embedded steels were recorded using embedded RE. For blocks with galvanic CP, both the electrochemical potential and the protective current supplied by the aluminum anode to the steel reinforcement were monitored. The potential of the aluminum anode is between −1050 mV and −1100 mV vs. Ag/AgCl/seawater at ambient temperature. The cathode-to-anode ratio is 4.9. For a reinforced concrete structure to be cathodically protected in passive and active stage, the cathode-to-anode ratio is reported to be 0.64 and 1.28, respectively [25]. The specimens in this study are prepared by embedding steel in concrete without chlorides. Therefore, the cathode-to-anode ratio 4.9 > 0.64 is sufficient for the intended study. Also, it is known that the corrosion experiments usually get disrupted due to the failure of electrical connections, only one anode (considering that it has sufficient cathode-to-anode ratio to protect the RC system), was connected to three RC blocks to reduce the risk of frequent failures associated with individual connections to anode. To measure current, a 10 Ω shunt resistor was connected to each RC block, allowing current monitoring via the potential drop across the resistor.

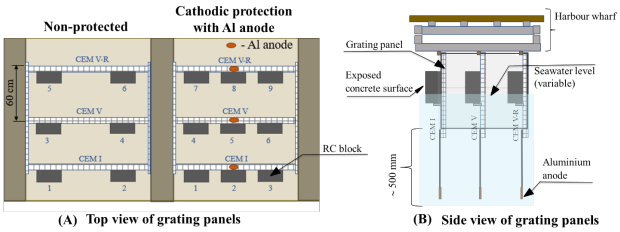

Figure 2. Schematic diagram of the layout of grating panels with RC blocks positioned beneath the harbour wharf in Banyuls-sur-Mer, France. Here, CEM I: RC blocks with smooth texture, CEM V with smooth and CEM V-R with rough texture.

3.3 Description of exposure site and conditions

The experimental arrangement was setup in mid-November 2023 at the exposure site in Mediterranean Sea near Banyuls-sur-Mer, France. This long-term study was supported by the regional technological REMIMED (Réseau Marin Instrumenté en MEDiterranée) platform at Banyuls-sur-mer, France. The temperature, atmospheric pressure, relative humidity, and salinity at this location were monitored every hour (not presented here). In addition, an ultrasonic water-level measurement sensor was installed to record the water level every 10 minutes. Then, this data was processed and presented relative to the height ($h = 20\ cm$) of the RC block. Following visual inspections of biofilm formation, the naturally formed biofilm on the surfaces of concrete exposed to seawater was carefully removed using a swab (to avoid damage to the concrete surface) on February 5, 2024, (approximately after 80 days of the installation setup). Note that the complete removal of biofilm on rough surface of concrete is not guaranteed due to its microscopic peaks and troughs.

4 Results and discussion

This section presents measurements (half-cell potential (HCP), mixed potential, and protection current) from the field experiment on RC blocks with CEM I and CEM V (smooth and rough texture) without and with galvanic CP. Mixed potential refers to the electrochemical potential measured for the coupled system (steel reinforcement and galvanic anode) against MnO_2 reference electrode. While protection current refers to the measured current supplied by the galvanic anode to steel reinforcement in mitigating corrosion. The effect of water level and biofilm development on corrosion characteristics of embedded steel are investigated and presented next. Note that the corrosion activity of steel in concrete described in this study, is specific to this geometry, exposure period, and environment. Therefore, the measured quantitative corrosion potentials and protection current may not be applicable to other configurations [26].

The HCP of steel in concrete without CP was monitored continuously for an interval of every 15 minutes over an exposure duration of 320 days for CEM I with smooth, CEM V with smooth and rough surface textures. The recorded HCP were relative to the MnO_2 RE. However, to facilitate easier comparison with the literature, they are presented in terms of the saturated Copper/Copper Sulfate Electrode (CSE).

Figure 3A shows the water level data for an exposure period of 320 days. The raw data obtained from the ultrasonic water level sensor corresponded to the height of the tides. This data was then fitted using a polynomial function, and the resulting interpolation was the water level variation with respect to the height of specimen. The water level (in cm) on Y axis is the water level with respect to the base of the specimen. The two red dashed lines indicate the base and top of the specimen. Therefore, water level of 0 indicates that the water level is at the base of the specimens and water level of 20 or more indicates that the specimens are submerged in seawater. Figure 3B and 3C show the HCP for CEM I with smooth texture, CEM V with smooth and rough texture vary from –300 to –850 mV_{CSE}, –200 to –400 mV_{CSE}, and –100 to –500 mV_{CSE}, respectively in the non-protected category. While some correlations are observable between water level and the measured potentials, it is difficult to infer meaningful conclusions from these. Therefore, data is presented differently to draw the relationship between water level and corrosion characteristics of embedded steel in concrete. There are some studies that have investigated the influence of internal relative humidity (RH) on the overall corrosion performance of RC [27]. Moreover, some simulations in a laboratory setup showed that the combined effects of external factors such as temperature, moisture content, and external RH modify the internal RH only on the surface region [28]. Andrade et al. [29] and references therein researched the effects of temperature, humidity, and rainfall on concrete in a field and determined that changes in temperature may prevent vapor pressure within the concrete to reach equilibrium. Note that the RC blocks in this study are placed very close to seawater level and ambient RH is always more than 80 %. In this situation, this study observes that even when relative humidity remains relatively consistent over time, variations in water level have a notable influence on the corrosion of embedded steel in concrete. This, in turn, bridges the gap by highlighting the influence of water level fluctuations on steel corrosion activity, which has received less attention. More on this will be presented later. Figure 3D, 3E, 3F, and 3G show the monitored mixed potential of embedded steels and anodes and protection current density (assumed uniform distribution on steel reinforcement) for steel embedded in CEM I (smooth texture), and CEM V concrete with smooth and rough texture, respectively with the variations in water level. The triplicate specimens for each cement type and surface texture consistently demonstrate the same trend over time, confirming the reproducibility of the observed patterns.

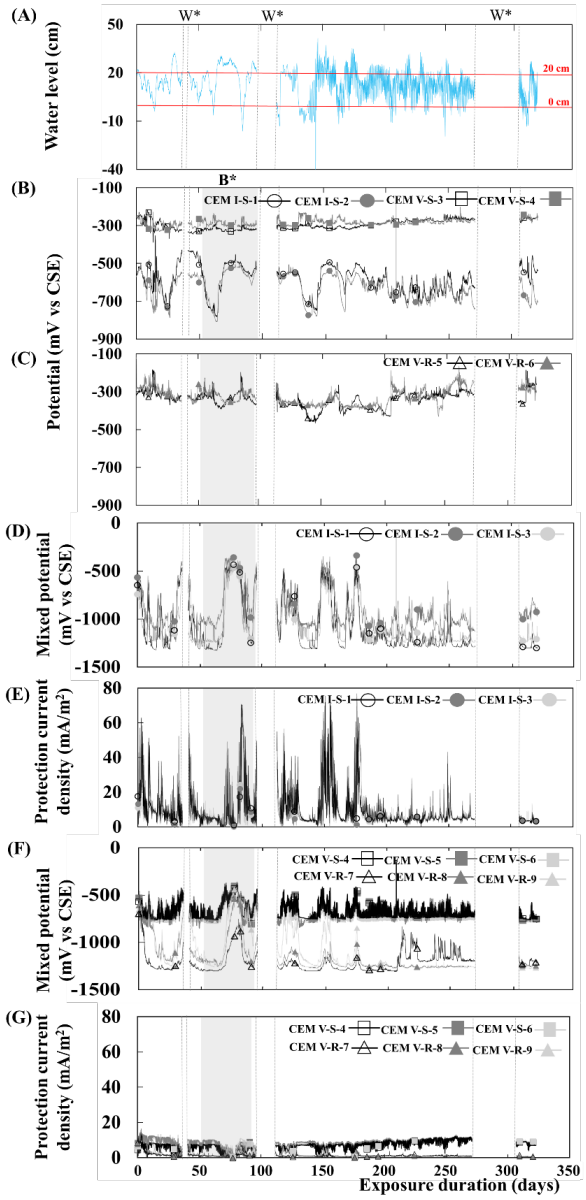

Figure 3. (A) Water level data relative to the specimen height of 20 cm; (B) HCP of steel embedded in CEM I and CEM V concrete with smooth texture, and (C) with rough texture recorded for RC without CP; Mixed potential (D, F) and protection current density (E, G) for CEM I and CEM V with both textures for galvanic CP; W*: exposure duration affected by power outages (no data in dashed sections) and B*: measurements before and after removal of biofilm and used to plot Figure 7.

4.1 Effect of water level and biofilm on corrosion characteristics of embedded steel in concrete

To better analyze the variations of HCP and water levels, the clustered HCPs of steel were analyzed for several intervals, such as 0-5, 5-10, 10-15, and 15-20 cm, ranging from 0 cm (base of the specimen) to 20 cm at the top. According to ASTM C876-22b, the HCP less than –350 mV_{CSE} indicate 90 % probability of corrosion in conventional concrete systems like OPC [30]. However, the standard and many literatures advise caution when interpreting these measures, especially in wet

environments, because moisture can affect HCP significantly. As a result, defining the HCP threshold indicative of active corrosion is difficult due to environmental sensitivity. Therefore, the HCPs in this research are analyzed in relative terms and not absolute thresholds.

Figure 4A, 4B, and 4C show the distribution of HCP over varying water levels relative to specimen height (cm) for CEM I with smooth, CEM V concrete with smooth and rough textures, respectively. The violins in the plots show that majority of measured HCPs of embedded steel reinforcement fall within the range of violin for the water level of interest. Additionally, the boxplot within the violin shows the distribution of HCPs. One unfilled marker within each scatter shows the median of all the measured HCPs. In Figure 4A, the measured HCP for CEM I concrete with smooth texture range is the same for all the water levels, but the distribution of HCPs is significantly different for water levels less than 15 cm and more than 15 cm. For less than 15 cm, the distribution of HCP has narrowed violins and more scatter of HCP between –400 and –800 $mV_{CSE.}$ Whereas HCPs for embedded steel in concrete with water levels more than 15 cm has wider violins and less scatter ranging from –450 to –600 mV_{CSE} of measured HCPs. The median of HCPs of embedded steel for water level <15 cm and >15 cm moves slightly to lesser negative potentials (–500 mV_{CSE} and –600 mV_{CSE}) - revealing that the corrosion characteristics of the steel-concrete interface are affected by changes in water levels. This might be attributed to the increased water saturation, with enhanced ionic conductivity and reduced oxygen availability [31]. These plots show the variation of measured HCPs with respect to water levels and even within the same water levels. Note that the distribution of HCPs in water levels less than 15 cm have two violins – indicating that there is large dispersion of data. This may be attributed to the quick change in water levels relative to the measurements collected by the sensor installed for collecting the data for water levels. On the other hand, when water levels are more than 15 cm, the HCPs are more stabilised than the remaining – which again could be attributed to the limited supply of oxygen to the steel surface due to the filling of pores with highly ionic conductive seawater. Authors envision that analysis of the collected big data can reveal better understanding of the corrosion of steel in the tidal zone, which is an ongoing project and is not presented here.

Figure 4B and 4C for CEM V with smooth and rough texture reveal lesser scatter fluctuations in measured HCP than CEM I concrete. It is most likely due to the higher concrete resistivity of CEM V, with less ionic conductivity and less diffusion of oxygen. While CEM V concrete with smooth and rough texture show more stable HCP in comparison to CEM I. This is due to the inclusion of SCMs such as fly ash and slag in CEM V cement. The presence of SCMs densifies the pore structure of the cement matrix, resulting in decreased ionic transport [32]. This appears to be a favorable influence on the microstructure of the cement matrix. Previous laboratory study has shown that HCP of steel in fly-ash-based concrete in 3 % NaCl solutions remains stable over time [33]. These results are consistent with those reported here in both textural variations for CEM V. Note that rough texture CEM V shows wider violins - indicating larger scatter in measured HCPs than that of CEM V with smooth texture. This could be attributed to more local water retention in the roughness of the concrete surface, further enhancing microbial colonization [34]. In other words, even if the sensor records a lower water level, the water is retained on the surface of concrete and affecting the corrosion activity of steel in CEM V rough.

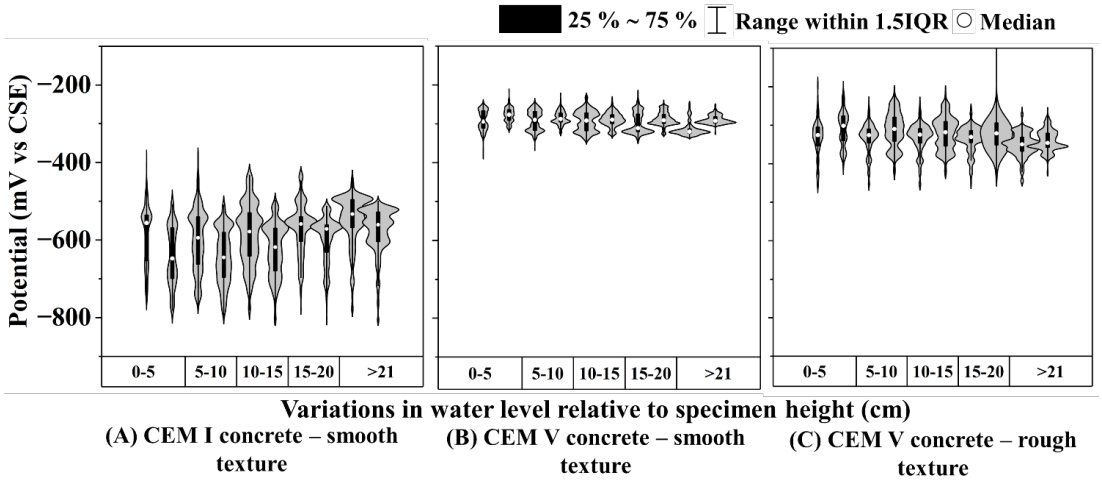

Figure 4. Distribution of measured half-cell potential of RC blocks with no CP for 320 days.

Another novel aspect of this research work is the identification of the effect of the presence of biofilm on the corrosion of embedded steel, which is not reported in the literature. For this, the HCPs are analysed under two conditions – the presence and absence of biofilm – at varying water levels. Please note the residual effects of biofilm on the concrete surface were not investigated in this study due to the strong wave action, contributing to periodic biofilm detachment. This natural phenomenon introduces variability that makes systematic assessment of biofilm formation and its long-term effects challenging. As such, this becomes a limitation of the current investigation. The selected electrochemical measurements were 25 days before and after biofilm removal. Figure 7 shows that the measured HCPs

for CEM I with biofilm have large scatter ranging from –400 to –800 mV_{CSE}. Whereas HCPs for CEM I without biofilm are more positive than the HCPs measured for embedded steel in CEM I concrete with less scatter for each of the water levels. The more negative HCPs with biofilm can be attributed to HCPs of steel with oxygen deficiency due to presence of biofilm. Yu et al. [35] have shown through laboratory studies that dissolved oxygen in seawater facilitates biofilm formation and maturation in the early stages while also limiting chloride ion penetration over a 120-day test period. When biofilm is removed, the oxygen is facilitated at steel surface leading to corrosion activities, and stable HCPs. Note that the formation of biofilm is a stepwise process, starting with the adsorption of inorganic molecules such as polysaccharides and proteins which condition the surface and results in a gelatinous layer on moist substrates [36]. In the tidal zone, the differences in moisture content over the exposed RC surface, results in uneven or heterogeneous biofilm development. For instance, Figure 5 shows the photograph of RC blocks partially submerged, revealing non-uniform biofilm development, mostly concentrated near the base of the RC block. Visual inspections revealed the development of macroalgae on RC surfaces. Further analysis using chlorophyll a (a standard method to quantify the chlorophyll a pigment found in algae) confirmed the presence of macroalgae (data not shown here). Macroalgae are aerobic biofilms with two metabolic functions, including photosynthesis during daylight, that produces oxygen as a byproduct, and cellular respiration that consumes oxygen. This creates a potential gradient in oxygen concentration that might probably occur within the biofilm, as well as influencing the concrete-biofilm interface [34], [37]. Hence, this aspect may affect the electrochemical characteristics of steel in concrete. There is negligible effect of biofilm on the measured HCPs of steel in concrete with CEM V (both texture). This could be attributed to refined pore structure of CEM V reducing the ingress of oxygen. Therefore, even with biofilm, the oxygen concentrations at steel surface will be low. The point to note is that the HCPs of steel in CEM V concrete is significantly more positive than the HCPs of steel embedded in CEM I, which is in line with the literature [33]. Also, the HCPs for steel in concretes with different binders are not advised to be compared with absolute number.

Figure 5. Photograph taken at the end of 250 days of exposure in the tidal zone, showing partially submerged RC blocks with non-uniform biofilm development, predominantly clustered towards the base.

4.2 Behaviour of galvanic anode CP under the influence of water level and biofilm

As per ISO 12696, the effectiveness of Al anode in CP for steel in concrete across two cement types is assessed using the electrochemical potential data [18]. To accomplish this, the initial potential of the reinforcement was monitored for 15 hours in CEM I with smooth texture, CEM V concrete with smooth and rough texture that ranged from -470 mV_{CSE} to -559 mV_{CSE}, -230 mV_{CSE} to -330 mV_{CSE}, and -287 mV_{CSE} to -422 mV_{CSE}, respectively before connection to the Al anode. Upon connection to Al anode, the polarization caused a shift towards a more negative potential in across all RC, ranging from -580 mV_{CSE} to -780 mV_{CSE}. This shows that the aluminum anode used in this study is providing efficient CP. The polarization resistance measurements were conducted after 56 days of curing for both CEM I and CEM V, and the results indicated 63.21 Ωm^2 for CEM I and 81.97 Ωm^2 for CEM V (current response measured during polarization test shown in Figure 6) [38]. This suggests that CEM V exhibits higher resistivity compared to CEM I. This difference in electrochemical behaviour hints at the less negative electrochemical potential shift upon connection to Al anode under the tested conditions. Moreover, the findings indicated that the shift in potential for steel embedded in CEM V concrete is less negative than in CEM I concrete, irrespective of texture. This difference in the corrosion potential range of rebar in both cement types may be due to local conditions such as the physical characteristics (porosity, fineness, etc.), chemical composition of the cement matrix, and initial electrochemical potential of reinforcement. Some of the investigations in the literature include the performance of aluminum-alloy (Al-Zn-In) anodes embedded in mortar containing 0.1 % Cl^- by cement mass that was investigated in lake water. Here, the anodes were connected to steel reinforcement in concrete piles located in tidal and splash zones. The findings indicate that the anode effectively protected the steel, that was reported to be -900 mV vs. $Cu/CuSO_4$ [39]. Another laboratory study investigated the external aluminum alloy-based anode connected to steel rebars submerged in 3.5 % NaCl solution. Their findings indicated that the anode used was more effective in preventing corrosion in passive steel than in actively corroding steel [40]. Additionally, the same authors claim that the offshore RC structures in the splash zone might be protected with galvanic CP, as done in this study. Figure 7 (bottom plots) show the distribution of protection current density in concrete for CEM I (smooth texture), (B) CEM V (smooth texture), and (C) CEM V (rough texture) for the cases with and without biofilms. Figure 7A, for CEM I concrete (smooth texture), “with biofilm” condition, water level intervals below 10 cm show extremely narrow violins, implying less scatter, whilst the base has slightly more. As water levels rise (say, 10-15 cm or higher) violins slightly broaden at the base, indicating a small increase in the variability in current density. However, current density remains low overall. The median barely reveals an upward trend. As water levels rise (>15 cm), biofilm continues acting as a barrier. The low protective current density is another

indicator. The absence of biofilm suggests that, irrespective of water level variations, the aluminum anode is generating higher average protection current than that generated in the presence of biofilm. At water levels above 15 cm, the violins clearly show broad bases, indicating a larger spread in protection current density. This is attributed to increased oxygen availability, further suggesting the good performance of anode. For CEM V concrete with smooth and rough texture, in the presence of biofilm, the average protection current range is broader, starting at 15 cm water level intervals. At the same time, the absence of biofilm indicates that the protection current is uniformly distributed within a range for smooth and rough texture specimens. It is important to note that the effectiveness of cathodic protection (CP) remains unaffected despite a minimal presence of biofilm on RC structures. However, the results from this study can be used to understand the qualitative information of various corrosion characteristics.

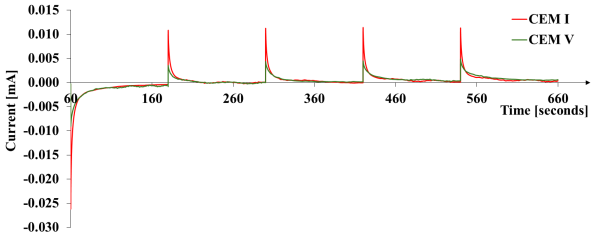

Figure 6. Current measured during the polarization test.

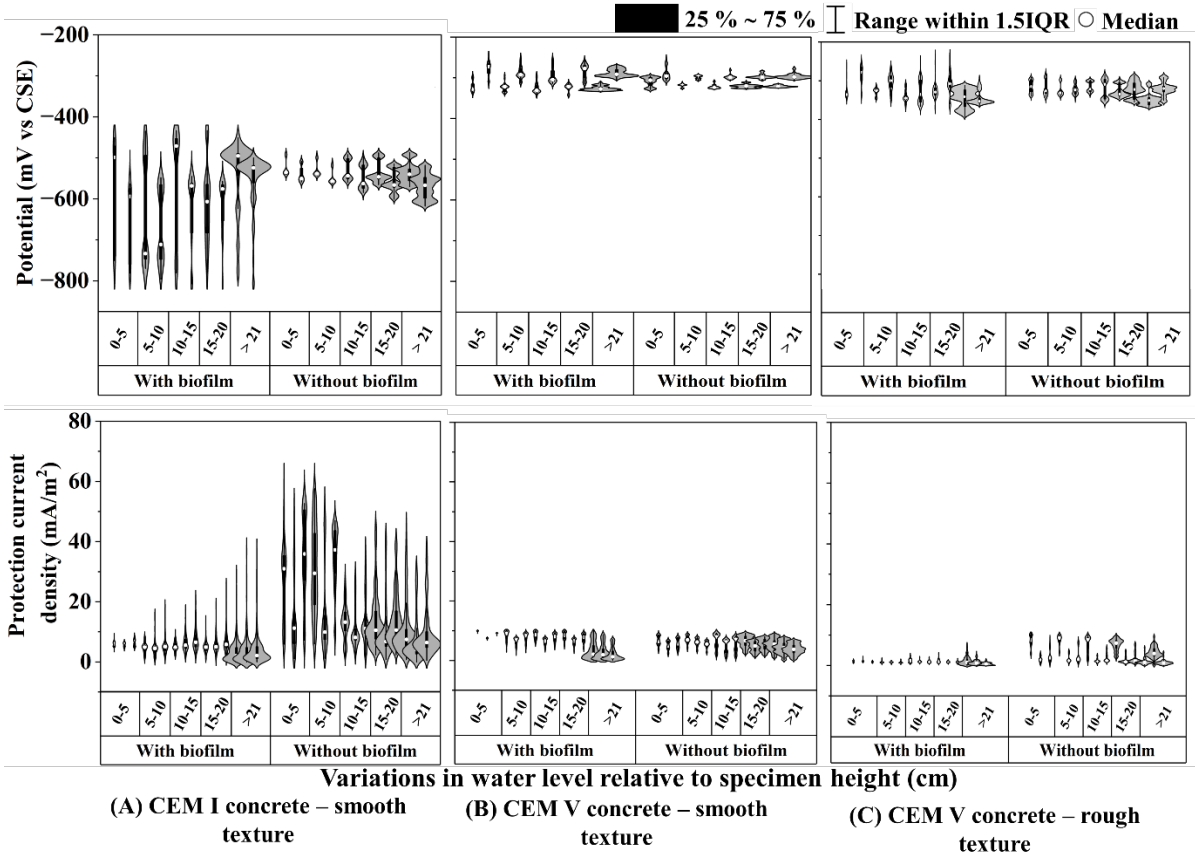

Figure 7. Distribution of half-cell potential for the non-protected category (top) and protection current for protected category (bottom) for RC blocks, recorded for 50 days (including a 25-day dataset for conditions with and without biofilm).

5 Conclusions

The 320-day field experiment on RC blocks in the tidal zone was conducted to evaluate the corrosion characteristics of steel embedded in concrete with CEM I and CEM V binders for two textures of the exposed surface of the latter, both with and without cathodic protection. For this, the electrochemical potential and protection current of steel in concrete in the case of galvanic CP were monitored continuously. These electrochemical characteristics were further correlated to water level and biofilm, to understand the variations in potentials. Moreover, the application of CEM I and CEM V provided useful insights into the behavior of steel embedded in concrete. This further allows us to determine which is better suited for marine environments in terms of durability. The results of corrosion characteristics of RC show that, both with and without CP, the biofilm serves as a physical barrier to the diffusion of oxygen. Biofilm influences the electrochemical behaviour of steel, as seen in the variations in protection current following biofilm removal leading to an increase in protection current, in extension, suggesting the efficient performance of Al anode. Additionally, the effect of the exposed surface's texture is highlighted, showing that smooth surface diffuses more oxygen and, consequently, has less negative potential. Thus, this study demonstrates the influence of surface texture and the physical barrier effect of biofilm. However, it is important to exercise caution here as the results are specific

to the conditions studied in this scenario and may vary under different environmental factors. The corrosion activity described here is liable to evolve over time as the results represent a small part of the long-term field testing of CP. Further research may focus on investigating the composition of biofilm as it is crucial in understanding the electrochemical reactions contributing to the electrochemical process on the surface of steel embedded in concrete.

Acknowledgements

The authors are grateful to the Region Occitanie for financial support (DuMaCoBio project), to the Wind'Occ agency for its federation and connection support during the construction and operation of the project, and to the Bio2Mar (K. Escoubeyrou) and Remimed technical platforms for providing services inclusive of instrumentation, vessels, and scuba diving service. The authors are grateful to RWE Company for its financial support. DK acknowledges the Chaire de professeur junior funding (ANR-23-CPJ1-0114-01) by Agence Nationale de la Recherche.

Authorship statement (CRediT)

Deeksha Margapuram: Writing – Original Draft, Data Curation, Validation, Investigation, Formal analysis, Conceptualization. **Marie Salgues**: Writing – Review & Editing, Supervision, Resources, Methodology, Project administration, Conceptualization. **Océane Thibault**: Methods. **Raphaël Lami**: Resources, Methodology, Project administration. **Benjamin Erable**: Resources, Methodology, Project administration. **Michel Groc**: Methodology, Resources, Conceptualization. **Renaud Vuillemin** : Resources, Investigation, Conceptualization. **Bruno Hesse** : Resources, Investigation, Methodology. **Jean-Claude Souche** : Resources, Investigation. **Florian Stratta**: Resources, Investigation. **Marine Bayle**: Resources, Investigation, Methodology. **Jean-Bernard Memet**: Resources, Methodology. **Laurent Zudaire**: Resources, Investigation, Methodology. **Fabrice Deby**: Writing – Review & Editing, Supervision. **Stéphane Laurens**: Resources, Conceptualization, Funding acquisition. **Chantal Chalhoub**: Methodology, Investigation, Software, Conceptualization, Resources. **Elie Sassine**: Methodology, Investigation, Conceptualization. **Fabien Nougarolles**: Resources, Investigation, Methodology. **Deepak Kumar Kamde**: Writing – Review & Editing, Visualization, Validation, Supervision, Conceptualization. **Alexandra Bertron**: Conceptualization, Methodology, Writing – Review & Editing, Supervision, Resources, Investigation, Project administration, Funding acquisition.

References

[1] M. Shafiee, "Failure analysis of spar buoy floating offshore wind turbine systems," Innov. Infrastruct. Solut., vol. 8, no. 1, p. 28, Jan. 2023. https://doi.org/10.1007/s41062-022-00982-x

[2] E. Baita-Saavedra et al., "An Economic Analysis of An Innovative Floating Offshore Wind Platform Built with Concrete: The SATH® Platform," Applied Sciences, vol. 10, no. 11, p. 3678, May 2020. https://doi.org/10.3390/app10113678

[3] A. Mathern, C. Von Der Haar, and S. Marx, "Concrete Support Structures for Offshore Wind Turbines: Current Status, Challenges, and Future Trends," Energies, vol. 14, no. 7, p. 1995, Apr. 2021. https://doi.org/10.3390/en14071995

[4] K. Li et al., "Long-term field exposure of structural concretes in marine environment: state-of-the-art review by RILEM TC 289-DCM," Mater Struct, vol. 55, no. 7, p. 205, Sep. 2022. https://doi.org/10.1617/s11527-022-02027-2

[5] Y. Yi, D. Zhu, S. Guo, Z. Zhang, and C. Shi, "A review on the deterioration and approaches to enhance the durability of concrete in the marine environment," Cement and Concrete Composites, vol. 113, p. 103695, Oct. 2020. https://doi.org/10.1016/j.cemconcomp.2020.103695

[6] M. Z. Y. Ting and Y. Yi, "Durability of cementitious materials in seawater environment: A review on chemical interactions, hardened-state properties and environmental factors," Construction and Building Materials, vol. 367, p. 130224, Feb. 2023. https://doi.org/10.1016/j.conbuildmat.2022.130224

[7] S.-J. Kwon, H.-S. Lee, S. Karthick, V. Saraswathy, and H.-M. Yang, "Long-term corrosion performance of blended cement concrete in the marine environment - A real-time study," Construction and Building Materials, vol. 154, pp. 349-360, Nov. 2017. https://doi.org/10.1016/j.conbuildmat.2017.07.237

[8] Margapuram, D. et al. (2025). Study of Early-Age Phenomena at the Concrete-Marine Biofilm Interface in Seawater for the Construction of Eco-Friendly Fowt's. In: Ferrara, L., Muciaccia, G., Trochoutsou, N. (eds) Proceedings of the RILEM Spring Convention and Conference 2024. RSCC 2024. RILEM Bookseries, vol 55. Springer, Cham. https://doi.org/10.1007/978-3-031-70277-8_37

[9] J. R. Bone, R. Stafford, A. E. Hall, and R. J. H. Herbert, "The intrinsic primary bioreceptivity of concrete in the coastal environment - A review," Developments in the Built Environment, vol. 10, p. 100078, May 2022. https://doi.org/10.1016/j.dibe.2022.100078

[10] D. Margapuram, "Short-term interactions of concrete, biofilm, and seawater in the submerged zone of marine environments for sustainable floating offshore wind turbines," Construction and Building Materials, 2024. https://doi.org/10.1016/j.conbuildmat.2024.138840

[11] M. Hayek, M. Salgues, J.-C. Souche, E. Cunge, C. Giraudel, and O. Paireau, "Influence of the Intrinsic Characteristics of Cementitious Materials on Biofouling in the Marine Environment," Sustainability, vol. 13, no. 5, p. 2625, Mar. 2021. https://doi.org/10.3390/su13052625

[12] T. K. L. Teong, "Marine bioreceptivity among green concretes," Ecological Engineering, 2024. https://doi.org/10.1016/j.ecoleng.2024.107284

[13] Q. Qu et al., "Corrosion behavior of cold rolled steel in artificial seawater in the presence of Bacillus subtilis C2," Corrosion Science, vol. 91, pp. 321-329, Feb. 2015. https://doi.org/10.1016/j.corsci.2014.11.032

[14] N. Guo et al., "Enhanced corrosion protection action of biofilms based on endogenous and exogenous bacterial cellulose," Corrosion Science, vol. 194, p. 109931, Jan. 2022. https://doi.org/10.1016/j.corsci.2021.109931

[15] G. Qiao, B. Guo, J. Ou, F. Xu, and Z. Li, "Numerical optimization of an impressed current cathodic protection system for reinforced concrete structures," Construction and Building Materials, vol. 119, pp. 260-267, Aug. 2016. https://doi.org/10.1016/j.conbuildmat.2016.05.012

[16] J. García-Contreras et al., "Effect of Cathodic Protection on Reinforced Concrete with Fly Ash Using Electrochemical Noise," Materials, vol. 14, no. 9, p. 2438, May 2021. https://doi.org/10.3390/ma14092438

[17] E. B. Muehlenkamp, M. D. Koretsky, and J. C. Westall, "Effect of Moisture on the Spatial Uniformity of Cathodic Protection of Steel in Reinforced Concrete," CORROSION, vol. 61, no. 6, pp. 519-533, Jun. 2005. https://doi.org/10.5006/1.3278188

[18] BSI (2012) BS EN ISO 12696:2012: Cathodic protection of steel in concrete. BSI, London, UK

[19] Definition of steel products, EN 10079:2007, 2007

[20] Steel for the reinforcement of concrete - Weldable reinforcing steel - General, NF EN 10080:2005, 2005

[21] Myrdal, R. (2014). The electrochemistry and characteristics of embeddable reference electrodes for concrete (Vol. 43). Woodhead Publishing

[22] AFNOR.2022. XP P18-481 : Essai sur béton durci - Mesure de la résistivité électrique
[23] AFNOR. 2022. NF P18-459 : Essai de Porosité et de Masse Volumique
[24] C09 Committee, Test Method for Electrical Indication of Concretes Ability to Resist Chloride Ion Penetration. https://doi.org/10.1520/C1202-12
[25] A. M. Hassanein, G. K. Glass, and N. R. Buenfeld, "Protection current distribution in reinforced concrete cathodic protection systems," Cement and Concrete Composites, vol. 24, no. 1, pp. 159-167, Feb. 2002. https://doi.org/10.1016/S0958-9465(01)00036-1
[26] S. Mundra et al., "Application of electrochemical methods for studying steel corrosion in alkali ‐ activated materials," Materials & Corrosion, vol. 74, no. 7, pp. 988-1008, Jul. 2023. https://doi.org/10.1002/maco.202313743
[27] J. N. Enevoldsen, C. M. Hansson, and B. B. Hope, "The influence of internal relative humidity on the rate of corrosion of steel embedded in concrete and mortar," Cement and Concrete Research, vol. 24, no. 7, pp. 1373-1382, 1994. https://doi.org/10.1016/0008-8846(94)90122-8
[28] D.-W. Ryu, J.-W. Ko, and T. Noguchi, "Effects of simulated environmental conditions on the internal relative humidity and relative moisture content distribution of exposed concrete," Cement and Concrete Composites, vol. 33, no. 1, pp. 142-153, Jan. 2011. https://doi.org/10.1016/j.cemconcomp.2010.09.009
[29] A. Andrade, J. Sarría, and C. Alonso, "Relative humidity in the interior of concrete exposed to natural and artificial weathering," Cement and Concrete Research, vol. 29, no. 8, pp. 1249-1259, Aug. 1999. https://doi.org/10.1016/S0008-8846(99)00123-4
[30] G01 Committee, Test Method for Corrosion Potentials of Uncoated Reinforcing Steel in Concrete. https://doi.org/10.1520/C0876-22B
[31] K. C. Liam, S. K. Roy, and D. O. North Wood, "Chloride ingress measurements and corrosion potential mapping study of a 24-year-old reinforced concrete jetty structure in a tropical marine environment," Magazine of Concrete Research, vol. 44, no. 160, pp. 205-215, Sep. 1992. https://doi.org/10.1680/macr.1992.44.160.205
[32] S. Uthaman, R. P. George, V. Vishwakarma, M. Harilal, and J. Philip, "Enhanced seawater corrosion resistance of reinforcement in nanophase modified fly ash concrete," Construction and Building Materials, vol. 221, pp. 232-243, Oct. 2019. https://doi.org/10.1016/j.conbuildmat.2019.06.070
[33] Y.-S. Choi, J.-G. Kim, and K.-M. Lee, "Corrosion behavior of steel bar embedded in fly ash concrete," Corrosion Science, vol. 48, no. 7, pp. 1733-1745, Jul. 2006. https://doi.org/10.1016/j.corsci.2005.05.019
[34] M. L. Neo, P. A. Todd, S. L.-M. Teo, and L. M. Chou, "Can artificial substrates enriched with crustose coralline algae enhance larval settlement and recruitment in the fluted giant clam (Tridacna squamosa)?," Hydrobiologia, vol. 625, no. 1, pp. 83-90, Jun. 2009, doi: 10.1007/s10750-008-9698-0. https://doi.org/10.1007/s10750-008-9698-0
[35] A. Yu, Q. Yuan, H. Rong, D. Liu, and Y. Feng, "Effects of dissolved oxygen on marine biofilm formation and its on microstructure and chloride ion permeability of concrete," Journal of Building Engineering, vol. 75, p. 107074, Sep. 2023. https://doi.org/10.1016/j.jobe.2023.107074
[36] A. Bertron, "Understanding interactions between cementitious materials and microorganisms: a key to sustainable and safe concrete structures in various contexts," Mater Struct, vol. 47, no. 11, pp. 1787-1806, Nov. 2014. https://doi.org/10.1617/s11527-014-0433-1
[37] A. De Beer, P. Stoodley, F. Roe, and Z. Lewandowski, "Effects of biofilm structures on oxygen distribution and mass transport," Biotech & Bioengineering, vol. 43, no. 11, pp. 1131-1138, May 1994. https://doi.org/10.1002/bit.260431118
[38] S. Laurens et al., "Steady-state polarization response of chloride-induced macrocell corrosion systems in steel reinforced concrete - numerical and experimental investigations," Cement and Concrete Research, vol. 79, pp. 272-290, Jan. 2016. https://doi.org/10.1016/j.cemconres.2015.09.021
[39] O. T. De Rincón, M. F. De Romero, A. R. De Carruyo, M. Sánchez, and J. Bravo, "Performance of sacrificial anodes to protect the splash zone of concrete piles," Mat. Struct., vol. 30, no. 9, pp. 556-560, Nov. 1997. https://doi.org/10.1007/BF02486400
[40] L. Bertolini, M. Gastaldi, M. Pedeferri, and E. Redaelli, "Prevention of steel corrosion in concrete exposed to seawater with submerged sacrificial anodes," Corrosion Science, vol. 44, no. 7, pp. 1497-1513, Jul. 2002. https://doi.org/10.1016/S0010-938X(01)00168-8